Inorg. Chem. **2005**, *44*, 3755–3761

Synthesis, Structure, and Thermal Properties of Soluble Hydrazinium Germanium(IV) and Tin(IV) Selenide Salts

David B. Mitzi

IBM T. J. Watson Research Center, P.O. Box 218, Yorktown Heights, New York 10598

Received December 8, 2004

The crystal structures of two hydrazinium-based germanium(IV) and tin(IV) selenide salts are determined. $(N_2H_5)_4Ge_2Se_6$ (**1**) [$I4_1cd$, $a = 12.708(1)$ Å, $c = 21.955(2)$ Å, $Z = 8$] and $(N_2H_4)_3(N_2H_5)_4Sn_2Se_6$ (**2**) [$P\bar{1}$, $a = 6.6475(6)$ Å, $b = 9.5474(9)$ Å, $c = 9.8830(10)$ Å, $\alpha = 94.110(2)°$, $\beta = 99.429(2)°$, $\gamma = 104.141(2)°$, $Z = 1$] each consist of anionic dimers of edge-sharing metal selenide tetrahedra, $M_2Se_6^{4-}$ (M = Ge or Sn), separated by hydrazinium cations and, for **2**, additional neutral hydrazine molecules. Substantial hydrogen bonding exists among the hydrazine/hydrazinium molecules as well as between the hydrazinium cations and the selenide anions. Whereas the previously reported tin(IV) sulfide system, $(N_2H_5)_4Sn_2S_6$, decomposes cleanly to microcrystalline SnS_2 when heated to 200 °C in an inert atmosphere, higher temperatures (>300 °C) are required to dissociate selenium from **1** and **2** for the analogous preparations of single-phase metal selenides. The metal chalcogenide salts are highly soluble in hydrazine, as well as in a variety of amines and DMSO, highlighting the potential usefulness of these compounds as precursors for the solution deposition of the corresponding metal chalcogenide films.

Introduction

The diverse structural chemistry and range of electronic properties exhibited by metal chalcogenides lead to important opportunities for these materials in contemporary electronic device research. Some of the earliest solar cells[1] and thin film field-effect transistors (TFTs)[2] were, in fact, based on metal chalcogenide active layers. More recent efforts on metal chalcogenides have focused on improved transistors,[3−7] solar cells,[8,9] and thermoelectric[10,11] and memory materials.[12−16] Commercial applications include optical disks based on antimony−germanium−telluride phase-change materials, which currently dominate the CD-RW and DVD markets.[16]

Most electronic applications of metal chalcogenides and other semiconductors depend on the ability to deposit continuous thin films with a well-defined thickness. Common deposition techniques for the chalcogenides routinely require relatively high deposition temperatures or vacuum conditions. Vapor-phase techniques involving vacuum processes, such as evaporation or sputtering,[17,18] and chemical vapor deposition[19,20] are commonly employed to deposit high-quality films for device applications. Although broadly applicable across the chalcogenide family, these techniques are not readily amenable to large area, low-cost deposition. In contrast, solution-based film deposition is particularly desirable

(1) Reynolds, D. C.; Leies, G.; Antes, L. L.; Marburger, R. E. *Phys. Rev.* **1954**, *96*, 533.
(2) Weimer, P. K. *Proc. IRE* **1962**, *50*, 1462.
(3) Gan, F. Y.; Shih, I. *IEEE Trans. Electron Devices* **2002**, *49*, 15.
(4) Meth, J. S.; Zane, S. G.; Sharp, K. G.; Agrawal, S. *Thin Solid Films* **2003**, *444*, 227.
(5) Ridley, B. A.; Nivi, B.; Jacobson, J. M. *Science* **1999**, *286*, 746.
(6) Duan, X.; Niu, C.; Sahi, V.; Chen, J.; Parce, J. W.; Empedocles, S.; Goldman, J. L. *Nature* **2003**, *425*, 274.
(7) Mitzi, D. B.; Kosbar, L. L.; Murray, C. E.; Copel, M.; Afzali, A. *Nature* **2004**, *428*, 299.
(8) Britt, J.; Ferekides, C. *Appl. Phys. Lett.* **1993**, *62*, 2851.
(9) Contreras, M. A.; Egaas, B.; Ramanathan, K.; Hiltner, J.; Swartzlander, A.; Hasoon, F.; Noufi, R. *Prog. Photovolt. Res. Appl.* **1999**, *7*, 311.
(10) Kim, Y.; DiVenere, A.; Wong, G. K. L.; Ketterson, J. B.; Cho, S.; Meyer, J. R. *J. Appl. Phys.* **2002**, *91*, 715.
(11) Sabo, Y. P. *J. Thermoelectr.* **2001**, *4*, 58.
(12) Kyratsi, T.; Chrissafis, K.; Wachter, J.; Paraskevopoulos, K. M.; Kanatzidis, M. G. *Adv. Mater.* **2003**, *15*, 1428.
(13) Terada, M.; Furuya, K.; Okamura, T.; Morimoto, I.; Nakao, M. *Jpn. J. Appl. Phys.* **1993**, *32*, 5219.
(14) Friedrich, I.; Weidenhof, V.; Njoroge, W.; Franz, P.; Wuttig, M. *J. Appl. Phys.* **2000**, *87*, 4130.
(15) Jongenelis, A. P. J. M.; Coombs, J. H.; van Es-Spiekman, W.; Jacobs, B. A. J. *J. Appl. Phys.* **1996**, *79*, 8349.
(16) (a) Ohta, T.; Nishiuchi, K.; Narumi, K.; Kitaoka, Y.; Ishibashi, H.; Yamada, N.; Kozaki, T. *Jpn. J. Appl. Phys., Part 1* **2000**, *39*, 770. (b) Ohta, T.; Yoshioka, K.; Isomura, H.; Akiyama, T.; Imanaka, R. *Proc. SPIE-Int. Soc. Opt. Eng.* **1995**, *2514*, 302.
(17) Van Calster, A.; Vervaet, A.; De Rycke, I.; De Baets, J. *J. Cryst. Growth* **1988**, *86*, 924.
(18) Chaiken, A.; Nauka, K.; Gibson, G. A.; Lee, H.; Yang, C. C.; Wu, J.; Ager, J. W.; Yu, K. M.; Walukiewicz, W. *J. Appl. Phys.* **2003**, *94*, 2390.
(19) Parkin, I. P.; Price, L. S.; Hibbert, T. G.; Molloy, K. C. *J. Mater. Chem.* **2001**, *11*, 1486.
(20) Sanchez-Juarez, A.; Ortíz, A. *Semicond. Sci. Technol.* **2002**, *17*, 931.

10.1021/ic048276l CCC: $30.25
Published on Web 04/19/2005

because of the possibility of using low-temperature, high-throughput (with potential for large area) processes such as spin coating, drop casting, printing, or stamping. However, the covalency of the extended metal chalcogenide framework generally leads to low solubility in common solvents.

Recently, we reported the deposition of high-quality, continuous, ultrathin (<10 unit cells thick) main-group metal chalcogenide films from hydrazine-based solutions of SnS_2 and $SnSe_2$.[7] The key to this process was the identification of hydrazine as a solvent and the incorporation of excess chalcogen (e.g., S or Se) in the solution, thereby enabling the formation of suitable highly soluble hydrazinium-based precursors [e.g., $(N_2H_5)_4Sn_2S_6$ and $(N_2H_4)_3(N_2H_5)_4Sn_2Se_6$]. Thin films of the precursors may be deposited by spin coating in air at room temperature, followed by a brief annealing step at < 300 °C (under inert atmosphere) to effect decomposition to the targeted metal chalcogenide film. The resulting films, incorporated as channel layers within TFTs, exhibit n-type field-effect mobilities >10 cm^2/V sec, approximately 1 order of magnitude higher than the mobilities of previous spin-coated channel layers (either n- or p-type). The structure and thermal properties of the tin(IV) sulfide precursor $(N_2H_5)_4Sn_2S_6$ have been previously reported.[7] Here, we report the preparation, detailed structure, and thermal properties of several analogous hydrazinium-based metal selenide precursors based on tin(IV) and germanium(IV) selenide anions.

Experimental Section

Synthesis. $(N_2H_5)_4Ge_2Se_6$ (1). A multiphase yellow product is obtained by reacting (under an inert nitrogen atmosphere) 2 mmol of $GeSe_2$ (0.461 g) and 2 mmol of Se (0.158 g) in 1 mL of freshly distilled hydrazine. **NOTE: hydrazine is highly toxic and should be handled using appropriate protective equipment to prevent contact with either the vapors or the liquid.** The reaction produces vigorous bubbling and rapidly yields a clear light-yellow solution. The solution is evaporated overnight to dryness under a N_2 flow and transferred into a drybox (where it is allowed to further dry in the drybox antichamber for several hours), yielding approximately 753 mg of a bright-yellow crystalline product. Chemical analysis yielded N(21.9%) and H(3.6%). Note that these values are more consistent with those calculated for $(N_2H_4)_3(N_2H_5)_4Ge_2Se_6$ [N(23.1%) and H(3.8%)] than with those for $(N_2H_5)_4Ge_2Se_6$ [N(14.9%) and H(2.7%)]. Indeed, powder X-ray diffraction (XRD) indicates a mixture of peaks from $(N_2H_5)_4Ge_2Se_6$ (**1**) (minor component), as well as (more predominantly) from a phase with similar lattice constants to that expected for $(N_2H_4)_3(N_2H_5)_4Sn_2Se_6$ (**2**). The diffraction pattern rapidly changes in air as the material loses hydrazine, ultimately yielding a more single-phase pattern consistent with that expected for **1**. A crystal was isolated for the hydrazine-rich phase, $(N_2H_4)_3(N_2H_5)_4Ge_2Se_6$, and the approximate triclinic lattice constants were determined to be $a = 6.597(2)$ Å, $b = 9.381(3)$ Å, $c = 9.745(3)$ Å, $\alpha = 93.67(1)°$, $\beta = 100.34(1)°$, and $\gamma = 104.97(1)°$ (i.e., similar to those for the Sn compound **2**—see Table 1). Although a full data set was collected and solved for $(N_2H_4)_3(N_2H_5)_4Ge_2Se_6$, confirming an isostructural relationship to **2**, the quality of this refinement was poor because of the rapid loss of hydrazine from the sample during data collection. From the mixed-phase sample, a single crystal of **1** was also selected for a full structure analysis (see Table 1).

Table 1. Crystallographic Data for $(N_2H_5)_4Ge_2Se_6$ (**1**) and $(N_2H_4)_3(N_2H_5)_4Sn_2Se_6$ (**2**)

chemical formula	$(N_2H_5)_4Ge_2Se_6$	$(N_2H_4)_3(N_2H_5)_4Sn_2Se_6$
fw	751.19	939.53
space group	$I4_1cd$ (No. 110)	$P\bar{1}$ (No. 2)
a, Å	12.708(1)	6.6475(6)
b, Å	12.708(1)	9.5474(9)
c, Å	21.955(2)	9.8830(10)
α, deg		94.110(2)
β, deg		99.429(2)
γ, deg		104.141(2)
V, Å^3	3545.6(5)	595.9(2)
Z	8	1
ρ_{calcd}, g/cm^3	2.814	2.618
wavelength, Å	0.71 073 (Mo Kα)	0.71 073 (Mo Kα)
abs coeff (μ), cm^{-1}	157.0	112.8
R_f[a]	1.92	2.30
R_w[b]	2.68	2.82

[a] $R_f = \Sigma(|F_o| - |F_c|)/\Sigma(|F_o|)$. [b] $R_w = [\Sigma w(|F_o| - |F_c|)^2/\Sigma(w|F_o|^2)]^{1/2}$.

$(N_2H_4)_3(N_2H_5)_4Sn_2Se_6$ (2). Yellow crystals of **2** are formed by dissolving (in a nitrogen atmosphere, over several minutes, with stirring) 0.277 g of $SnSe_2$ (1 mmol) in 1 mL of hydrazine and 0.079 g of Se (1 mmol), yielding, ultimately, a light-yellow solution. Evaporating the solution under flowing nitrogen gas over a period of several hours leads to the formation of approximately 0.450 g of a yellow crystalline powder (96% yield). The powder loses weight while sitting on a balance at room temperature, reflecting a loss of solvent (i.e., hydrazine) from within the structure. Chemical analysis, observed: N(20.8%), H(3.5%). Calcd: N(20.9%), H(3.4%).

X-ray Crystallography. A pale-yellow blocklike crystal of $(N_2H_5)_4Ge_2Se_6$ (**1**) [$(N_2H_4)_3(N_2H_5)_4Sn_2Se_6$ (**2**)], with the approximate dimensions 0.03 mm × 0.05 mm × 0.18 mm [0.11 mm × 0.12 mm × 0.46 mm], was selected under a microscope and attached to the end of a quartz fiber with five-minute epoxy. Intensity data were collected with a Bruker SMART CCD diffractometer equipped with a fine focus 2.4 kW sealed tube X-ray source (Mo Kα radiation). The data were collected at room temperature using an exposure time of 60 s [6 s] per frame. For **2**, a relatively short collection time was employed to minimize hydrazine loss from the sample during data collection.

Final cell parameters (Table 1) and a crystal orientation matrix were obtained by a least-squares fit of 4526 [3504] reflections. An empirical absorption correction based on equivalent reflections was applied to the intensity data.[21] The structure was solved and refined using the NRCVAX 386 PC version program.[22] First, the Ge [Sn] and Se atoms were located using direct methods. The N atoms were then located using successive Fourier difference maps. All heavy atoms (Ge, Sn, Se, and N) were refined anisotropically. Hydrogen atoms were located from difference maps and fully refined using isotropic thermal parameters. The minimum and maximum peaks in the final difference Fourier map correspond to −0.4 and 0.5 e/Å^3 [−0.6 and 0.6 e/Å^3]. No additional symmetry was detected for the refined structures using the MISSYM program.[23] For **1**, refinement yielded a flack parameter of −0.02(8). Crystallographic results for the two compounds are summarized in Table 1. Selected bond lengths and angles for each of the compounds are given in Table 2. A complete listing of crystallographic data (in CIF format) is given in the Supporting Information.

Powder X-ray Diffraction. XRD powder patterns were collected for thermogravimetric analysis (TGA) products using a Siemens

(21) Sheldrick, G. M. *SADABS*; Institut für Anorganische Chemie der Universität Göttingen: Göttingen, Germany, 1997.
(22) Gabe, E. J.; Le Page, Y.; Charland, J.-P.; Lee, F. L.; White, P. S. *J. Appl. Crystallogr.* **1989**, *22*, 384.
(23) Le Page, Y. *J. Appl. Crystallogr.* **1988**, *21*, 983.

Table 2. Selected Bond Distances (Å) and Angles (deg) for **1** and **2**

$(N_2H_5)_4Ge_2Se_6$ (**1**)		$(N_2H_4)_3(N_2H_5)_4Sn_2Se_6$ (**2**)	
Ge1−Se1	2.415(3)	Sn−Se1	2.4609(5)
Ge1−Se1[a]	2.415(3)	Sn−Se2	2.5933(5)
Ge1−Se3	2.316(3)	Sn−Se2[b]	2.5909(4)
Ge1−Se3[a]	2.316(3)	Sn−Se3	2.4639(5)
Ge2−Se1	2.424(3)	Se2−Sn[b]	2.5909(4)
Ge2−Se1[a]	2.424(3)	N1−N2	1.434(6)
Ge2−Se2	2.305(3)	N3−N4	1.439(6)
Ge2−Se2[a]	2.305(3)	N5−N6	1.426(6)
N1−N2	1.450(7)	N7−N7[c]	1.462(8)
N3−N4	1.43(2)	Se1−Sn−Se2	110.64(2)
Ge1−Se1−Ge2	85.1(1)	Se1−Sn−Se2[b]	110.78(2)
Se1−Ge1−Se1[a]	95.2(2)	Se1−Sn−Se3	116.36(2)
Se1−Ge1−Se3	110.64(5)	Se2−Sn−Se2[b]	95.59(1)
Se1−Ge1−Se3[a]	110.82(5)	Se2−Sn−Se3	110.40(2)
Se1a−Ge1−Se3[a]	110.64(5)	Se2−Sn−Se3[b]	111.16(2)
Se3−Ge1−Se3[a]	116.7(2)	Sn−Se2−Sn[b]	84.41(1)
Se1−Ge2−Se1[a]	94.7(2)		
Se1−Ge2−Se2	110.55(5)		
Se1−Ge2−Se2[a]	111.78(5)		
Se2−Ge2−Se2[a]	115.6(2)		

[a] $1-x, -y, z$. [b] $1-x, 1-y, 1-z$. [c] $-x, -y, -z$.

D5000 diffractometer (Cu Kα radiation). The specimen for analysis was prepared by pressing powder of the sample into vacuum grease on a glass slide. No attempt was made to control preferred-orientation effects. The phases present were identified (e.g., $SnSe_2$, $GeSe_2$, Se) by comparison with powder diffraction file (PDF) cards or, in the case of the new compound $(N_2H_5)_4Sn_2Se_6$, by comparison with the calculated powder pattern for the analogous compound $(N_2H_5)_4Ge_2Se_6$ (**1**). In cases where a refinement of lattice constants was performed from the diffraction data [for $GeSe_2$, see Figure 7b; for $(N_2H_5)_4Sn_2Se_6$, see Figure 6a], initial cell constants from the PDF card (for $GeSe_2$) or from **1** [for $(N_2H_5)_4Sn_2Se_6$] were used. A Pawley refinement[24] was used to optimize the pattern parameters using the Accelrys MS Modeling package. The peak profiles were fitted using a pseudo-Voigt function. The final Pawley refinement R_{wp} values were 8.05% for the $(N_2H_5)_4Sn_2Se_6$ data and 5.52% for the $GeSe_2$ data.

Thermal Analysis. TGA scans were performed in a flowing nitrogen atmosphere at 2 °C/min using a TA Instruments TGA-2950 system.

Results and Discussion

Solution Processibility. While the solvent properties of hydrazine have long been of interest,[25] little solubility has been noted for the metal chalcogenides (although sulfur itself was reported to be highly soluble). Polysulfide- and polyselenide-based hydrazine hydrate solutions have, in fact, been used to precipitate transition and main-group metal chalcogenides,[26] using the corresponding solutions of the metal salts to effect the precipitation. In the current study, hydrazine is being used as a solvent for the metal chalcogenide systems, rather than as a precipitation medium. The differences come in the metal chalcogenides being considered (i.e., primarily main-group metal systems), the relatively concentrated hydrazine solvent employed, and the addition of extra chalcogen to the hydrazine to facilitate the formation of the soluble precursor.

The soluble hydrazinium MSe_2 (M = Ge or Sn) precursors are isolated by stirring metal(IV) selenide and selenium in hydrazine under ambient conditions. Dissolution primarily occurs through the overall reaction:

$$5N_2H_4 + 2Se + 2MSe_2 \rightarrow N_2 + 4N_2H_5^+ + M_2Se_6^{4-} \quad (1)$$

The pale-yellow color of each solution suggests the presence of at most a low concentration of polychalcogenide anions[27] and vigorous bubbling during dissolution supports the gas generation indicated in eq 1. Evaporation of the solution over a 24 h period yields the hydrazinium precursor crystals. Thin films of the precursor can similarly be prepared by spin coating the solution onto a suitable substrate.[7]

Although in our earlier studies of film deposition[7] we generated the hydrazinium precursor in situ during a spin-coating process (from a hydrazine solution), the precursor can also be isolated in crystalline form independent from the spin-coating process (as done in the current study). This enables the identification of other solvents for the precursor, rather than relying on the highly toxic and explosive hydrazine as a spin-coating solvent. We have recently shown, for example, that an indium(III) selenide precursor can be dissolved in an ethanolamine/dimethyl sulfoxide mixture.[28] The solutions formed using alternative (non-hydrazine-based) solvents may be useful for processing films, with the choice of solvent governed by the nature of the substrate surface (e.g., hydrophilic or hydrophobic) and the film composition/grain morphology desired. Although **1** and **2** are highly soluble in hydrazine, alternative solvents identified for these systems include amine-based solvents such as butylamine, ethylenediamine, and 3-methoxypropylamine, as well as dimethyl sulfoxide. Precursor **1**, for example, readily dissolves within a few minutes (at room temperature, with stirring) to form a clear yellow solution in each of the amine-based solvents listed above at a ∼0.5 M concentration (higher concentrations are likely also possible, although this was not addressed in the current study). DMSO solutions of **1** have also been prepared at the ∼0.1 M concentration level (dissolution takes several hours with stirring at room temperature). The resulting solutions appear to be stable for at least several days (longer time periods were not considered in this study) under inert atmosphere conditions.

Crystal Structures. Each of the title metal chalcogenide precursors consist of discrete $M_2Se_6^{4-}$ (M = Sn, Ge) anions of edge-sharing MSe_4 tetrahedra, as previously found for $(N_2H_5)_4Sn_2S_6$.[7] For $(N_2H_5)_4Ge_2Se_6$ (**1**) (Figure 1), the $Ge_2Se_6^{4-}$ anions have longer Ge−Se bridging [2.415(3)−2.424(3) Å] bonds than terminal [2.305(3)−2.316(3) Å] bonds and have Se−Ge−Se bond angles ranging from 94.7(2)° to 116.7(2)° (Table 2). These bond lengths and angles are in good agreement with the corresponding values observed for the $Ge_2Se_6^{4-}$ moiety in $Na_4Ge_2Se_6 \cdot 16H_2O$.[29]

(24) Pawley, G. S. *J. Appl. Crystllogr.* **1981**, *14*, 357.
(25) Welsh, T. W. B.; Broderson, H. J. *J. Am. Chem. Soc.* **1915**, *37*, 816.
(26) (a) Davies, D. A.; Vecht, A.; Silver, J.; Marsh, P. J.; Rose, J. A. *J. Electrochem. Soc.* **2000**, *147*, 765. (b) Marsh, P. J.; Davies, D. A.; Silver, J.; Smith, D. W.; Withnall, R.; Vecht, A. *J. Electrochem. Soc.* **2001**, *148*, D89.
(27) Bonnaterre, R.; Cauquis, G. *J. Chem. Soc., Chem. Commun.* **1972**, 293.
(28) Mitzi, D. B.; Copel, M.; Chey, S. J. *Adv. Mater.* **2005**, in press.
(29) Krebs, B.; Müller, H. *Z. Anorg. Allg. Chem.* **1983**, *496*, 47.

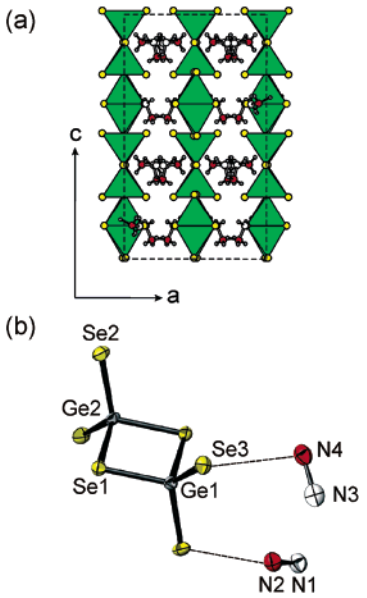

Figure 1. (a) Crystal structure of $(N_2H_5)_4Ge_2Se_6$ (**1**), viewed down the [010] direction (shown in polyhedral representation). Dashed lines indicate the unit cell outline. For clarity, atoms are represented as spheres, with uniform sizes selected for each atom type. Within the hydrazinium cations, the NH_3^+ nitrogen is depicted as a red-filled sphere, whereas the NH_2 nitrogen is depicted as an unfilled sphere. Hydrogen atoms are shown as small gray-filled spheres. (b) The detailed structure of the $Ge_2Se_6^{4-}$ anion and $NH_2NH_3^+$ cations (with atom labeling shown). For clarity, the hydrogen atoms have been removed. The thermal ellipsoids for Ge, Se, and N atoms are drawn at 50% probability.

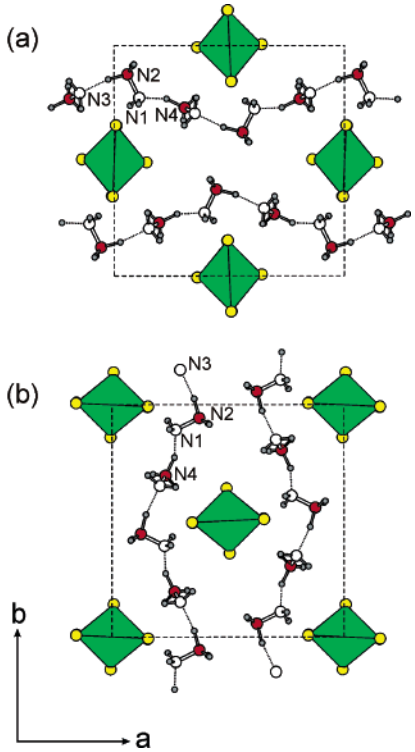

Figure 2. Parts a and b: Two successive layers (*ab* plane) progressing along [001], cut from the crystal structure for **1** (see Figure 1a). The $Ge_2Se_6^{4-}$ anion is shown in polyhedral representation. Dashed lines indicate the unit cell outline. Dotted lines indicate hydrogen bonding between neighboring hydrazinium cations. Within the hydrazinium cations, the NH_3^+ nitrogen is depicted as a red-filled sphere, whereas the NH_2 nitrogen is depicted as an unfilled sphere. Hydrogen atoms are shown as small gray-filled spheres.

The isolated $Ge_2Se_6^{4-}$ anions are charge balanced by a network of hydrazinium cations. The cations form extended hydrogen-bonded chains of repeating −N3···H−N2−N1···H−N4−N3··· lengths, which extend alternatively (progressing down the *c* axis) along the [100] or the [010] direction and weave among the $Ge_2Se_6^{4-}$ anions to form charge-balanced layers (Figure 2). Analogous hydrogen-bonded chains have been observed in $(N_2H_5)Cl$, $(N_2H_5)HC_2O_4$, and $(N_2H_5)H_2PO_4$,[30−32] with hydrogen bonding extending from the NH_3^+ group of one cation to the NH_2 group of a neighboring cation. The hydrogen-bonding distances (distances between nitrogens) for **1**, N3···H−N2 [2.84(1) Å] and N1···H−N4 [2.85(1) Å], are relatively short compared to the previously reported values for the reported hydrazinium-based compounds (2.87−3.14 Å).[30−32] In addition to the relatively strong hydrogen bonding among the hydrazinium cations, significant interaction between selenium atoms and the NH_3^+ groups of the hydrazinium cations is also noted, with short Se···H−N distances (Se to N) that include Se3···H−N2 [3.31(1) Å], Se3···H−N4 [3.35(1) Å], and Se2···H−N2 [3.32(1) Å]. The Se···H−N angles for these contacts fall in the range 161−172° (reasonable for hydrogen-bonding interactions), and Se-to-N distances are all shorter than those observed for Se···H−N hydrogen bonding in $[Mn(C_2H_8N_2)_3]_2Sb_2Se_5$ and $(H_3NC_2H_4NH_2)_3SbSe_4$ (3.40−3.67 Å).[33] These short selenium−nitrogen interactions are principally between hydrazinium cations in one layer (as shown in Figure 2) and $Ge_2Se_6^{4-}$ anions in an adjacent layer, thereby binding the layers together into a more three-dimensional structure.

For $(N_2H_4)_3(N_2H_5)_4Sn_2Se_6$ (**2**), the structure (Figure 3) consists of dimers of edge-sharing tin(IV) selenide tetrahedra, similar to the germanium analogue, with Sn−Se bond lengths of 2.4609(5)/2.4639(5) (Sn−Se1/Sn−Se3) Å for the two terminal bonds and 2.5909(4)/2.5933(5) Å for the two bridging Sn−Se2 bonds (Table 2). The observed Sn−Se distances, as well as the intradimer Sn···Sn interaction [3.4827(5) Å], are in good agreement with other compounds comprised of $Sn_2Se_6^{4-}$ anions.[34,35] The $Sn_2Se_6^{4-}$ anions are separated by both neutral hydrazine molecules and monoprotonated hydrazinium cations. The structure (Figure 3a) can nominally be considered as comprised of layers of $Sn_2Se_6^{4-}$ anions (extending in the *ac* plane), sandwiched on both sides by layers of hydrazinium cations. Incorporated between the electrically neutral cation−anion−cation sandwich structures are single layers of neutral hydrazine molecules. The N−N distances are typical for hydrazine species, with slightly shorter (though the difference is only marginally statistically significant) average bond distances

(30) Sakurai, K.; Tomiie, Y. *Acta Crystallogr.* **1952**, *5*, 293.
(31) Nilsson, A.; Liminga, R.; Olovsson, I. *Acta Chem. Scand.* **1968**, *22*, 719.
(32) Liminga, R. *Acta Chem. Scand.* **1965**, *19*, 1629.
(33) (a) Näther, C.; Wendland, F.; Bensch, W. *Acta Crystallogr., Sect E* **2003**, *59*, m119. (b) Wendland, F.; Näther, C.; Schur, M.; Bensch, W. *Z. Naturforsch.* **1998**, *53b*, 1144.
(34) Eisenmann, B.; Hansa, J. *Z. Kristallogr.* **1993**, *203*, 299.
(35) Krebs, B.; Uhlen, H. *Z. Anorg. Allg. Chem.* **1987**, *549*, 35.

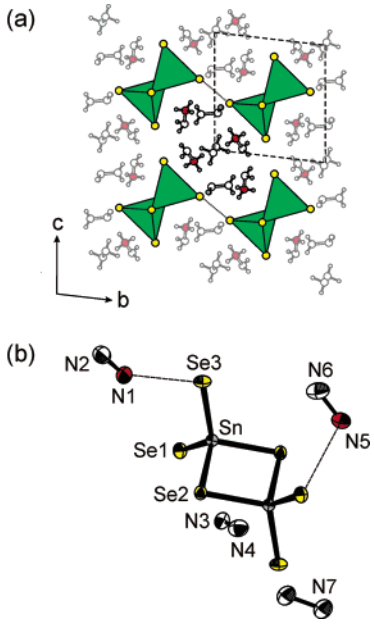

Figure 3. (a) Crystal structure of $(N_2H_4)_3(N_2H_5)_4Sn_2Se_6$ (**2**), viewed down the [100] direction (shown in polyhedral representation). Dashed lines indicate the unit cell outline. For clarity, atoms are represented as spheres, with uniform sizes selected for each atom type. Within the hydrazinium cations, the NH_3^+ nitrogen is depicted as a red-filled sphere, whereas the NH_2 nitrogen is depicted as an unfilled sphere. Hydrogen atoms are shown as small gray-filled spheres. The dotted lines indicate short Se1···Se1 interactions between layers of anions. The hydrazinium cations to be depicted in Figure 4 are highlighted (darker lines). (b) The detailed structure of the $Sn_2Se_6^{4-}$ anion, the NH_2NH_2 molecules, and the $NH_2NH_3^+$ cations (with atom labeling shown). For clarity, the hydrogen atoms have been removed. The thermal ellipsoids for Sn, Se, and N atoms are drawn at 50% probability.

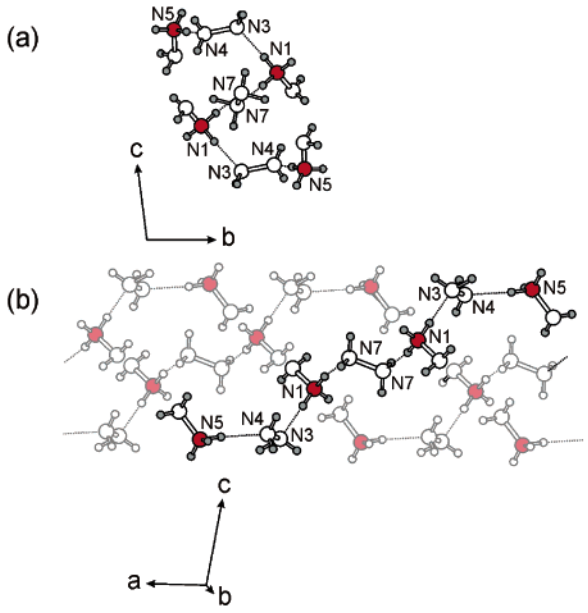

Figure 4. Two views of the hydrogen bonding (dotted lines) among hydrazinium cations in **2** (a) viewed along [100] (as in Figure 3) and (b) viewed approximately along [010]. Within the hydrazinium cations, the NH_3^+ nitrogen is depicted as a red-filled sphere, whereas the NH_2 nitrogen is depicted as an unfilled sphere. Hydrogen atoms are shown as small gray-filled spheres. In part b, a single hydrogen-bonded heptamer of hydrazinium cations is highlighted.

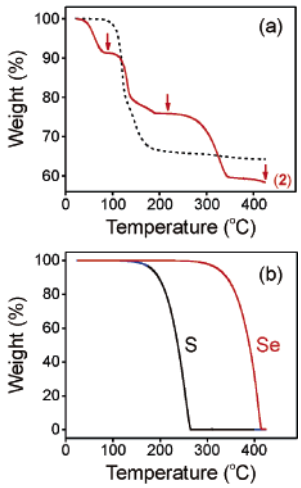

Figure 5. (a) TGA of the precursors $(N_2H_5)_4Sn_2S_6$ (dashed black line; from ref 7) and **2** (solid red line; 2 °C/min ramp rate, flowing nitrogen). The arrows mark the points along the decomposition pathway for which an XRD pattern was taken (see Figure 6). (b) TGA scans for sulfur and selenium, run under the same conditions as for the hydrazinium precursors.

for the cationic species [1.426(6) and 1.434(6) Å] compared to those for the neutral molecule [1.439(6) and 1.462(8) Å].

The neutral hydrazine molecules are held within the structure by hydrogen bonding to adjacent hydrazinium cations (Figure 4). Alternating hydrazinium cations and hydrazine molecules form hydrogen-bonded heptamers, N6−N5···H−N4−N3···H−N1−H···N7−N7···H−N1−H···N3−N4−H···N5−N6, which form short, twisted chains among the $Sn_2Se_6^{4-}$ anions (Figure 4). The relatively short hydrogen-bonding distances (distances between nitrogens) for **2**—N5−H···N4 [2.87(1) Å], N3···H−N1 [2.81(1) Å], and N1−H···N7 [2.81(1) Å]—are similar to the values observed in compound **1**. In addition to hydrogen bonding among the hydrazinium cations, there are also significant hydrogen-bonding interactions between selenium atoms and the NH_3^+ groups of the hydrazinium cations, with Se···H−N distances (Se to N) that include Se1···H−N5 [3.38(1) Å], Se3···H−N1 [3.45(1) Å], and Se3···H−N5 [3.44(1) Å]. These values are slightly longer than the corresponding distances obtained for **1**. A short Se1···Se1 interaction [3.493(1) Å] is also present among $Sn_2Se_6^{4-}$ moieties (Figure 3). This distance is significantly less than twice the ionic[36] or van der Waals[37] radius for Se (~3.8 Å).

Thermal Analysis. An important feature of the hydrazinium-based precursors, with respect to their use in the solution deposition of metal chalcogenide semiconductors, is the low temperature at which the precursors decompose. For $(N_2H_5)_4Sn_2S_6$, decomposition in an inert nitrogen atmosphere is essentially completed by 200 °C (Figure 5a).[7] The observed 34.6% weight loss (at 300 °C) is in good agreement with the expected value (34.9%) for the formation of SnS_2 (through the loss of four hydrazines and two hydrogen sulfides or their decomposition products). Decomposition of the analogous selenium-based precursor, **2**, occurs in several steps (Figure 5a). The first transition begins as early as room temperature and is complete by approximately 90 °C, with the observed weight change (−8.7%) in agreement with the loss of three hydrazines from **2** (−10.2% expected). The

(36) Shannon, R. D. *Acta Crystallogr., Sect. A* **1976**, *32*, 751.
(37) Bondi, A. *J. Phys. Chem.* **1964**, *68*, 441.

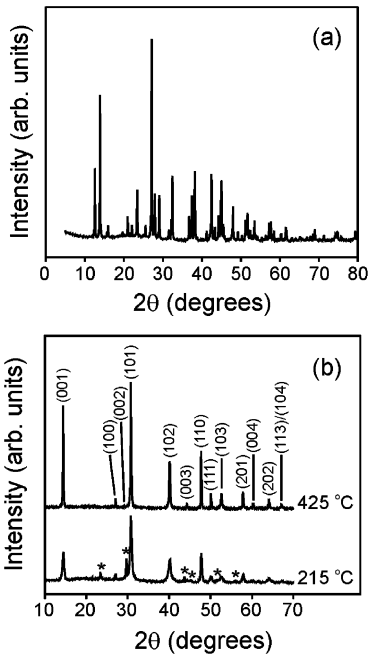

Figure 6. Powder XRD patterns (Cu Kα radiation) for precursor **2** after heating to (a) 90 °C and (b) 215 or 425 °C (using the same conditions as those for the TGA scans, see Figure 5a). Indexing of the powder pattern for the $(N_2H_5)_4Sn_2Se_6$ product in part a is given in the Supporting Information (i.e., *h*, *k*, *l*, *d* spacing, normalized intensities), as determined by Pawley refinement. The reflection indices given above the 425 °C data in part b are those for the $SnSe_2$ structure.[40] The asterisks in the 215 °C data indicate the reflection positions for elemental Se (PDF 06-0362).

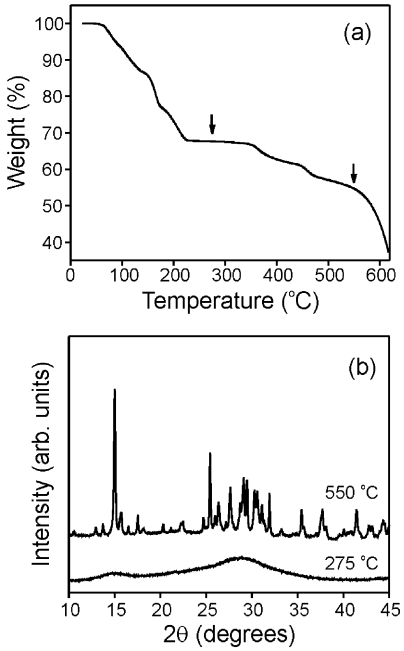

Figure 7. (a) TGA of the $GeSe_2$ precursor (2 °C/min ramp rate, flowing nitrogen). The arrows mark the points along the decomposition pathway for which an XRD pattern was taken (275 and 550 °C). (b) Powder XRD patterns (Cu Kα radiation) for the $GeSe_2$ hydrazinium precursor after heating to 275 and 550 °C (using the same conditions as those for the TGA scans). The diffraction pattern in part b (550 °C curve) matches that of $GeSe_2$ (PDF 30-0595). A Pawley refinement of the parameters for this pattern yielded a monoclinic cell with a = 7.0126(2) Å, b = 16.8341(6) Å, c = 11.8297(6) Å, and β = 90.729(1)°.

resulting product is isostructural with **1** (Figure 6a), with refined tetragonal lattice constants a = 12.775(1) Å and c = 22.705(1) Å. The slightly larger cell volume for $(N_2H_5)_4Sn_2Se_6$ compared with that of $(N_2H_5)_4Ge_2Se_6$ (**1**) (3705.5 versus 3545.6 Å^3) is consistent with the larger atomic radius of Sn. The chemical analysis of the product is also in good agreement with that expected for $(N_2H_5)_4Sn_2Se_6$—expected (N: 13.29%, H: 2.39%), found (N: 13.3%, H: 2.3%). The second transition, complete by approximately 200 °C, corresponds to a total weight change of approximately −24.2%, in good agreement with the weight change expected for the loss of four more hydrazine molecules from **2** (−23.9%, including the weight loss from the first transition). As for the decomposition of the sulfide system $(N_2H_5)_4Sn_2S_6$,[7] the transition to crystalline $SnSe_2$ is completed by ∼200 °C (i.e., see the XRD pattern in Figure 6b, 215 °C curve). In contrast to $(N_2H_5)_4Sn_2S_6$, however, for which the hydrazinium cation decomposes/dissociates from the sample at essentially the same temperature as the corresponding sulfide anion (presumably as hydrazine and hydrogen sulfide or their decomposition products), in **2** selenium remains in the sample after the loss of the hydrazinium species, as is evident from the XRD pattern in Figure 6b (215 °C curve). Note that hydrogen chalcogenides can decompose to hydrogen and chalcogen at moderate temperatures,[38] and metal chalcogenides may act to catalyze this reaction.[39] For **2**, the third major weight loss transition, which is complete by approximately 350 °C (yielding a total loss of −40.9% by 400 °C), corresponds to the loss of the two seleniums to yield $SnSe_2$ (total expected weight loss for the three transition ∼ −41.1%). As indicated in Figure 6b (425 °C curve), the resulting product is phase-pure crystalline $SnSe_2$ (CdI_2 structure type).[40] The lower volatility of selenium relative to sulfur (Figure 5b) implies that a higher temperature is required to achieve a clean sample of the targeted semiconductor (i.e., to lose the extra elemental selenium) relative to the decomposition of $(N_2H_5)_4Sn_2S_6$.

Decomposition of the germanium selenide precursor (Figure 7) is complicated by the fact that the as-prepared bulk precursor is not single phase but, rather, a mixture of **1** with a majority hydrazine-rich phase [i.e., $(N_2H_4)_3(N_2H_5)_4Ge_2Se_6$, a compound isostructural to **2**], as described in the Experimental Section. Furthermore, in contrast to the thermal decomposition of **2**, for which there is a small temperature region over which the hydrazine-depleted phase $(N_2H_5)_4Sn_2Se_6$ is stable, for the mixture of **1** and $(N_2H_4)_3(N_2H_5)_4Ge_2Se_6$, no significant plateau corresponding to **1** appears in the weight loss versus temperature data, making it difficult to prepare a single-phase sample of **1** via thermal decomposition (at least under the conditions examined). The decomposition pathway is also different in the sense that, although the decomposition of hydrazine from the sample appears to be complete by approximately 200 °C (as for **2**), the product obtained upon this decomposition appears to be amorphous (Figure 7b, 275 °C curve). Furthermore, the excess selenium

(38) Pearson, R. K.; Haugen, G. R. *Int. J. Hydrogen Energy* **1981**, *6*, 509.
(39) Chivers, T.; Lau, C. *Int. J. Hydrogen Energy* **1987**, *12*, 235.
(40) Busch, G.; Fröhlich, C.; Hulliger, F.; Steigmeier, E. *Helv. Phys. Acta* **1961**, *34*, 359.

that must remain in the sample at this stage of decomposition proves much more difficult to remove from the sample than for **2** and requires treatment at higher temperatures. Nevertheless, at temperatures above 500 °C, a single-phase product of $GeSe_2$ is achieved (Figure 7b, 550 °C curve). The total weight loss at 550 °C, 45.3%, is approximately what would be expected for the decomposition of $(N_2H_4)_3(N_2H_5)_4Ge_2Se_6$ to $GeSe_2$, consistent with the observation from the chemical analysis and powder XRD that this is the majority phase in the as-prepared germanium selenide precursor. Note that at temperatures above 550 °C, the $GeSe_2$ product sublimes. Therefore, a small fraction of the observed weight loss at 550 °C may already be attributed to this sublimation. Given the higher temperatures required for decomposition, the hydrazinium-based $GeSe_2$ precursor appears to be less well-suited for use as a convenient spin-coatable metal chalcogenide precursor (compared with the SnS_2 and $SnSe_2$ systems).

Conclusion

Two new hydrazinium-based germanium(IV) (**1**) and tin(IV) (**2**) selenide systems have been discussed. Each structure is found to consist of very similar $M_2Se_6^{4-}$ (M = Ge or Sn) anions interspersed with hydrazinium cations and, in the case of **2**, additional neutral hydrazine molecules. Each is stabilized by a range of bonding interactions, including relatively strong hydrogen bonding among the hydrazinium cations and hydrazine molecules, as well as among the hydrazinium cations and the $M_2Se_6^{4-}$ anions. Additionally, for compound **2**, a short Se···Se distance among anions indicates a further stabilizing interaction. The hydrazinium cations (and hydrazine molecules) dissociate from the structure upon heating in an inert atmosphere by approximately 200 °C. For the selenides, **1** and **2**, however, temperatures > 300 °C (especially for the Ge-based **1**) are required to achieve a phase-pure crystalline metal chalcogenide product [in contrast to the situation for $(N_2H_5)_4Sn_2S_6$], as a result of the higher temperature required to dissociate the excess selenium. Each of the ionic structures is highly soluble in hydrazine, as well as a range of other solvents, including amines and DMSO. As such, they are potentially useful as precursors for spin coating or solution processing metal chalcogenide films. In fact, for the tin(IV) chalcogenide systems, high-quality films have already been demonstrated and used as channel layers for TFTs.[7]

In a more general sense, the proposed solution-processing technique for metal chalcogenides[7] relies on the formation of a precursor that (1) has the extended metal chalcogenide framework broken up into smaller inorganic anions (enhancing solubility) and (2) has a countercation that is volatile and small enough for low-temperature removal from the film with minimal disruption (thereby enabling convenient recovery of the extended semiconducting framework after spin coating). It, therefore, seems likely that the hydrazinium precursor approach will be extendable beyond the hydrazinium-based germanium(IV) and tin(IV) systems described here, as well as to a wider range of solvent systems. We have recently demonstrated, for example, that high-quality In_2Se_3 films can be deposited using an indium selenide-based hydrazinium precursor dissolved in an ethanolamine/dimethyl sulfoxide (DMSO) mixed solvent.[28] The resulting high-quality In_2Se_3 films have proven useful as TFT channel layers, yielding mobilities as high as 16 cm^2/V sec. Furthermore, preliminary results have also yielded Sb_2S_3 and Sb_2Se_3 films,[7] spin coated from hydrazine-based solutions. So far, the facile formation and characterization of soluble hydrazinium-based precursors has been primarily limited to main-group metal chalcogenides. Corresponding initial attempts with several transition-metal-based chalcogenides (e.g., Cu_2Se, CdSe) have not been successful, as a result of the limited solubility of these systems in the hydrazine solvent under analogous conditions to those employed for the main-group metal systems.

Acknowledgment. The author thanks A. Afzali for distilling the hydrazine used in this study.

Supporting Information Available: An X-ray crystallographic file, in CIF format, containing information for $(N_2H_4)_3(N_2H_5)_4Sn_2Se_6$ and $(N_2H_5)_4Ge_2Se_6$. Table of observed XRD peaks for $(N_2H_5)_4Sn_2Se_6$, including indexing and normalized peak intensities. This material is available free of charge via the Internet at http://pubs.acs.org.

IC048276L